Available online at www.sciencedirect.com
ScienceDirect
Surface & Coatings Technology 201 (2007) 7924–7931
SURFACE & COATINGS TECHNOLOGY
www.elsevier.com/locate/surfcoat

Study of solidification behavior and splat morphology of vacuum plasma sprayed Ti alloy by computational modeling and experimental results

H.R. Salimijazi *, M. Raessi, J. Mostaghimi, T.W. Coyle

Centre for Advanced Coating Technologies, University of Toronto, Canada

Received 18 December 2006; accepted in revised form 20 March 2007
Available online 30 March 2007

Abstract

The microstructure of Ti–6Al–4V alloy manufactured by vacuum plasma spraying consists of individual lamellae, inter-lamellae boundaries, and porosity. Mechanical properties of the as-sprayed structure depend mainly upon the solidification behavior and resultant microstructure and morphology of the individual splats and cohesion between splats. Using a three-dimensional numerical model, the cooling rate and solidification behavior of a single Ti–6Al–4V droplet (50 μm) impacting on a titanium substrate under vacuum plasma spray conditions were investigated. Results were verified with experimental observations in single splats and as-sprayed microstructures obtained by vacuum plasma sprayed form of Ti–6Al–4V alloy. The average cooling rate of a single splat obtained from the numerical simulation was on the order of 10^8 °C/s and the solidification front velocity was approximately 63 cm/s which is in the range of the rapid solidification. The thickness of the splat was calculated to be around 3 μm and the deposition efficiency was approximately 70%. These results illustrated good agreements with those obtained from experiments.

Keywords: Vacuum plasma spraying; Near-net-shape forming; Ti–6Al–4V alloy; Solidification; Cooling rate; Single splat

1. Introduction

Titanium alloys have been used in the aerospace industry for more than three decades due to their superior properties such as specific strength, resistance to corrosion and oxidation, and fatigue strength. Their unique combination of properties has increased demand for the alloys in biomedical, automotive, and power generation applications. One of the most widely used titanium alloys is Ti–6Al–4V alloy. Engineering components of the alloy are conventionally manufactured by casting, forging, and powder metallurgy processes. Unfortunately, a high reactivity, relatively high cost, and low mechanical properties of the conventionally manufactured alloy have limited the number of its applications. Near-net-shape forming is a promising alternative to the conventional manufacturing processes. A growing need for new materials, high mechanical performance, and complex shaped structures has made near-net-shape forming among the most attractive manufacturing processes. Among various types of near-net-shape forming methods, vacuum plasma spray forming (VPSF) is one of the advanced techniques capable of forming reactive materials. In VPSF all manufacturing steps, such as melting, molding, casting, solidification, and machining are combined in a single step. In this process, powder particles of titanium alloy (+25/−45 μm) are injected into a dc plasma torch. The temperature of the core of the plasma jet is greater than 8000 °C. Gas velocity in the plasma spray torch can be varied from subsonic to supersonic using converging–diverging nozzles (between 600 m s^{-1} with pure Ar and 2300 m s^{-1} with Ar–H_2). Then the injected powders are melted and accelerated towards the substrate or mandrel where the molten particles impact, flatten and solidify. The deposition is built up by layering of splats. Thus, plasma sprayed deposits consist of individual splats (10^7–10^8 particles/s) which are connected together by mechanical and chemical bonding. The inter-lamellae boundaries are associated with a significant level of micro cracks and pores. Fig. 1 shows micrographs from a cross section of the sprayed form Ti–6Al–4V alloy. Lamellae are clearly observed in the etched microstructure. Microstructural development in VPSF

* Corresponding author.
E-mail address: jazi@mie.utoronto.ca (H.R. Salimijazi).

0257-8972/$ - see front matter © 2007 Elsevier B.V. All rights reserved.
doi:10.1016/j.surfcoat.2007.03.037

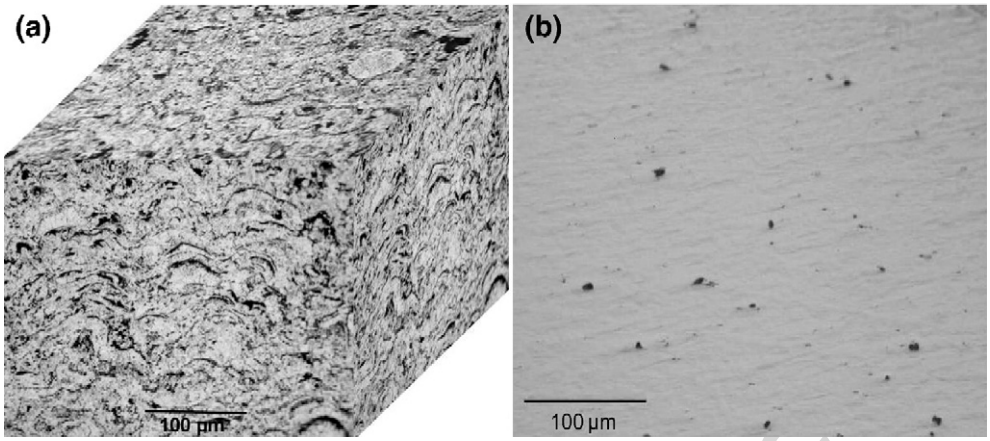

Fig. 1. Optical micrographs of (a) etched and (b) unetched from cross section of the VPSF Ti–6Al–4V alloy.

structures mainly depends on the solidification of individual splats and their position in the deposit. Although earlier models by Safai and Herman [1] for solidification of individual splats suggested a brick wall grain structure for the core region of the splat, more recent models of internal splat structure proposed by Mehrabian and Cohen [2,3] and developed by Sampath [4] confirm columnar grain structures in the core region of the splat oriented towards the heat transfer direction.

Thermal spray deposit properties mainly depend on the solidification and morphology of individual splats after solidification, cohesion between splats and adhesion between splats and substrates. The form of splats after solidification has been shown to be a function of droplet characteristics, such as in-flight particle size, velocity, temperature, and surface tension and also substrate temperature, surface morphology, thermal conductivity, surface clearance and thermal contact resistance between the splat and substrate. Knowledge of these relationships should permit optimization of deposition conditions to achieve optimum deposit properties and efficiency in VPSF.

In the present study, the solidification behavior of Ti–6Al–4V alloy under vacuum plasma spray forming conditions was investigated using both numerical simulation and experimental observations of single splats and as-sprayed structures. To predict the final morphology, cooling rate, solidification behavior, and deposition efficiency of individual splats of Ti–6Al–4V alloy under vacuum plasma spray forming condition, a three-dimensional model of free-surface fluid flow of droplet impact and solidification developed by Bussmann et al. [5] and Pasandideh-Fard et al. [6] have been employed. The model has been validated and discussed in detail in previous publications [5–8]. The model solves the mass, momentum and energy conservation equations, discretized using a finite volume technique on a three-dimensional, Eulerian structured grid. Fluid flow was assumed to be Newtonian, laminar and incompressible. The Volume-of-Fluid (VOF) algorithm was used to track the free surface of the droplet. Surface tension was incorporated as a component of the body force acting on the fluid-free surface using the Continuum Surface Force (CSF) model [9]. An adiabatic boundary condition was applied at the droplet-free surface. Simulation results were compared with observations in experiments conducted on Ti–6Al–4V in this study as well as results from other research groups.

In the experimental procedure of this study, the vacuum plasma sprayed form Ti–6Al–4V alloy was made by deposition of a standard feedstock Ti–6Al–4V powders (+45/−63 μm) produced by PyroGenesis Inc. (Montreal, Canada) using a vacuum plasma spraying process. An F4VB plasma gun from Plasma-Tecknik (Luzern, Switzerland) was used in a low-

Table 1
Vacuum plasma spray process parameters

Gun	F4VB, Plasma-Tecknik
Current, A	800
Total gas flow rate, (Ar, H_2, He), slpm	60
Secondary gas proportion, (H_2, He), %	30
Powder carrier gas (Ar), slpm	2
Feed rate, g/min	30
Chamber pressure, mbar	140
Spray distance, mm	300
Substrate temperature (°C)	800

Table 2
Data used for the numerical simulation of a Ti–6Al–4V molten droplet

Physical property	Value	Reference
Initial splat temperature (K)	1873[a]	
Substrate temperature (K)	1073[a]	
Melting point temperature (K)	1873	[10]
Latent heat of fusion (kJ kg^{-1})	440[b]	[10]
Kinematic viscosity of liquid (m^2s^{-1})	3×10^{-7}[b]	[10]
Thermal conductivity of liquid (J m^{-1} s^{-1} K^{-1})	30[b]	
Thermal conductivity of solid (J m^{-1} s^{-1} K^{-1})	3.1	[10]
Thermal conductivity of substrate (J m^{-1} s^{-1} K^{-1})	33.1	[10]
Specific heat of solid (J kg^{-1} K^{-1})	854.1	[10]
Specific heat of liquid (J kg^{-1} K^{-1})	989.2[b]	
Specific heat of substrate (J kg^{-1} K^{-1})	854.1	[10]
Density of liquid metal (kg m^{-3})	4120[b]	
Density of solid metal (kg m^{-3})	4500	[10]
Surface tension (N m^{-1})	1.2[b]	[10]
Velocity of particle (m s^{-1})	500[a]	
Diameter of particle (μm)	50[a]	

[a]Measured values from experiments were used.
[b]Values for commercially pure titanium were used.

pressure controlled atmosphere chamber. The temperature of the substrate and the prior deposit layer were maintained at approximately 800 °C. The typical vacuum plasma spray process parameters are summarized in Table 1. A DPV-2000 system from Tecnar Ltd (Montreal, Canada) was employed inside the vacuum chamber to measure the in-flight particles temperature and velocity upon the impact. The average temperature and velocity of the particles in the centre of the plasma plume upon the impact were approximately 1700 °C and 500 m s^{-1}.

2. Results and discussion

2.1. Numerical results

We simulated impact and solidification of a 50 μm diameter Ti–6Al–4V alloy droplet, initially at 1600 °C, onto a polished surface of Ti–6Al–4V alloy substrate whose temperature is kept constant at 800 °C. Based on experimental observations, the impact velocity was set to 500 m s^{-1}. Only a quarter segment of the droplet was simulated to save the computation time, and the

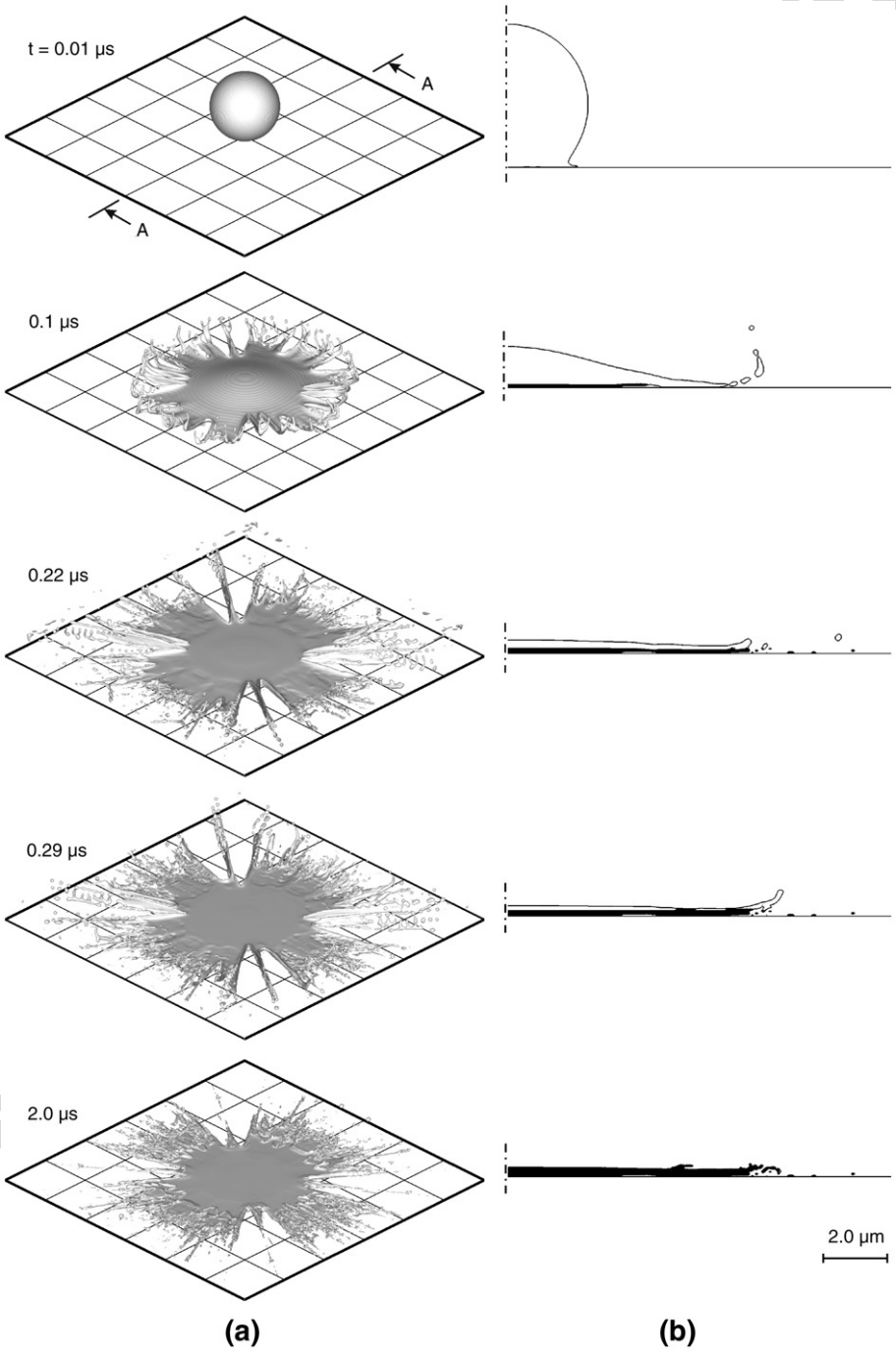

Fig. 2. (a) Computer generated images of a 50 μm diameter Ti–6Al–4V alloy droplet at 1600 °C impacting with a velocity of 500 m s^{-1} onto a titanium substrate at 800 °C. (b) A-A cross section of the droplet at the corresponding times. Solid phase is shown in black.

entire droplet was reconstructed by reflecting the results about planes of symmetry. The mesh size was chosen to be 1/40 of the droplet radius (0.625 μm). Previous experiences [6–8] showed that predicted droplet shapes do not change significantly when the computational grid is made smaller than 1/20 of the droplet radius. However, smaller grid resolution was chosen to accurately calculate the temperature distribution within the splat, which is the main focus of this study, and to know precisely the splat thickness. Thermal and physical properties of the molten Ti–6Al–4V alloy and Ti substrate used in the calculations are given in Table 2. The physical and thermal properties of the molten material and substrate were assumed to be constant and independent on temperature. Since molten Ti alloy is in contact with its own solid (complete wetting), the contact angle was set to zero. The model also requires a value for thermal contact resistance at the droplet–substrate interface. The contact resistance was assumed to be zero which means maximum heat transfer between the droplet and the substrate. This can be a realistic assumption because of complete wetting and having a polished, contaminant-free surface. The numerical computation was performed on an AMD Athlon 1.4 GHz PC and the CPU time was 340 h.

Fig. 2(a) shows sequences of the numerical simulation of Ti–6Al–4V alloy droplet during successive stages of impact, flattening, and solidification. Fig. 2(b) illustrates the A-A cross section of the spreading droplet at the corresponding times. Due to symmetry only half of the cross section is presented. The solid and liquid portions of the drop are shown in black and white, respectively. The time measured from the moment of impact is indicated next to each frame. Immediately after impact, the droplet is flattened and spread out in the radial direction. A thin layer of the drop, which is in contact with the substrate, is solidified during spreading (see Fig. 2(b) at 0.1 μs). The residual liquid jets out over the periphery of the bottom layer of the solidified liquid. This radial flow of liquid becomes unstable because of small variations in the liquid velocity and, eventually disintegrates into fingers at the edge of the drop which has already been

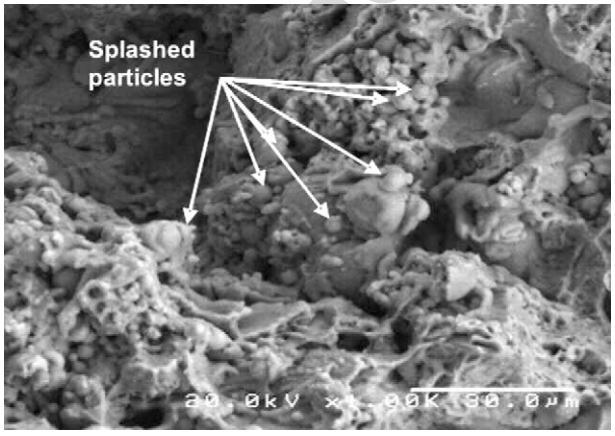

Fig. 3. A fracture surface of the as-sprayed Ti–6Al–4V alloy showing splashed particles.

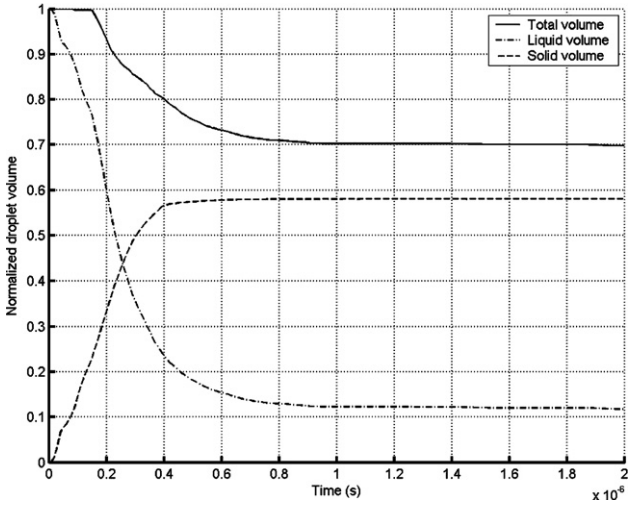

Fig. 4. Calculated total volume of the droplet and the volumes of liquid and solid phases all normalized by initial droplet volume versus time.

solidified (see Fig. 2(a) at 0.1 and 0.22 μs). These fingers finally detach to form satellite droplets, resulting in a so-called "splashing" phenomenon. These small droplets solidify during splashing and land on the substrate or prior deposit resulting in formation of weakly adhered solidified fine droplets around the bulk of the splats. The splashed particles, which reduce the cohesion of coatings, can be seen in the fracture surface of the as-sprayed structure (see Fig. 3) from the experiments conducted in this study.

Fig. 4 illustrates the total calculated volume of the droplet and the volumes of liquid and solid phases as a function of time. The volumes are all normalized by the initial volume of the droplet. The initial sharp increase in the solid volume is due to formation of a thin layer of solid in contact with the cold substrate during spreading. The subsequent reduction in solidification rate at approximately 0.08 μs after impact is due to the latent heat released by the thin solid film. Approximately 30% of the droplet material is lost due to splashing which starts around 0.18 μs after impact, when the major part of solidification happens. The thickness of the splat is measured from the numerical results (see Fig. 2(b) at 2 μs) and it is approximately 3 μm in the central region of the splat.

Fig. 5 presents the calculated droplet temperature versus time at various positions within the splat after impact. Point 1 is the centre of the impact near the splat/substrate interface. As expected, it experiences a sharp temperature decrease after impact. Points 2 and 3 are located 1.5 and 3 μm above the centre of impact, respectively, meaning that point 2 is on the mid plane of the splat and point 3 is on the top surface of the splat. The average temperature of the splat is also depicted in this figure. Since the solid/liquid interface acts as a planar heat source (interface-controlled heat transfer) while moving through the splat, the cooling rates change discontinuously at the solidification point. The slope change which occurs at 0.08 μs on the near substrate–splat interface curve is due to formation of a thin layer of solid on the substrate. Because of the latent heat release due to solidification, the cooling rate at point 1 decreases after

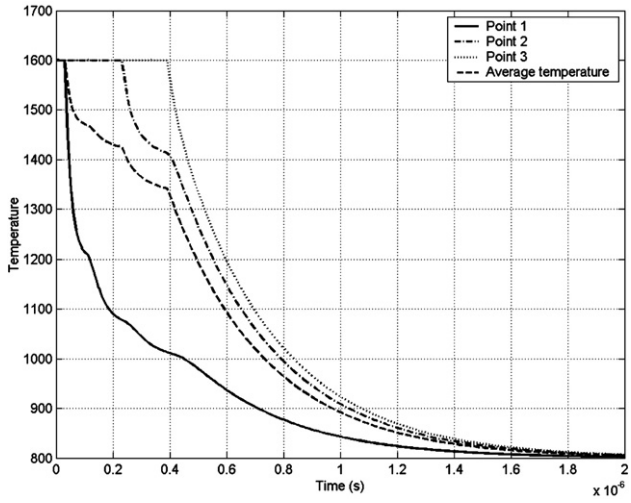

Fig. 5. Calculated droplet temperature at the centre of impact (point 1), mid point of the splat (point 2), top surface of the splat (point 3), and the average temperature of the splat.

0.08 μs. The solid/liquid interface passes through the mid point of the splat at around 0.23 μs and it finally reaches the top surface of the splat at 0.4 μs and solidification is complete. The solidified splat cools down to the substrate temperature at 2 μs. Next, the cooling rate is derived from the temperature history curves.

2.2. Average splat cooling and solidification rates

The rate of change of the average splat temperature is fairly representative of the cooling process in most cases. Ruhl [14] reported that the average cooling rate can be estimated from the initial splat temperature, T_t, to the half-temperature, $T_{1/2}$, where $T_{1/2} = \frac{1}{2}(T_t + T_s)$ and T_s is the substrate temperature. The half-temperature of splat can be calculated to be 1200 °C. Having the splat cooling time equal to 2 μs, the calculated average cooling rate to the half-temperature is approximately 2×10^8 °C/s. The average cooling rate estimated from the curve of the average temperature of the splat shown in Fig. 5 is 4×10^8 °C/s which is in good agreement with the cooling rate obtained from the half-temperature assumption.

The relationship between the cooling rate, Q, and heat transfer coefficient, h, for Newtonian cooling conditions can be expressed as [4]:

$$Q = \frac{h(T_t - T_s)}{\rho C_p d} \tag{1}$$

where h is the heat transfer coefficient (W/m^2 K), ρ is the density of the splat (kg m^{-3}), C_p is the specific heat capacity of the splat, (J kg^{-1} K), d is the splat thickness (m), and T_t and T_s are the splat and substrate temperatures, respectively. The calculated cooling rate from Newtonian cooling condition for a Ti–6Al–4V droplet is on the order of 10^8 °C/s. The cooling rates are also in the range of the calculated and measured cooling rates for single splats of different metallic materials formed under plasma spray condition [4,11–15]. The average cooling rate for splat solidification indicates rapid solidification during thermal spraying. Small variations in the cooling rates can arise due to differences in the thermal conductivity, initial temperature, and surface morphology of substrate, thermal contact resistance at substrate/splat interface, and thermal spray process parameters. The presence of entrapped air and micro cracks can also reduce the cooling rate. A void is clearly seen to be formed approximately 30 μm

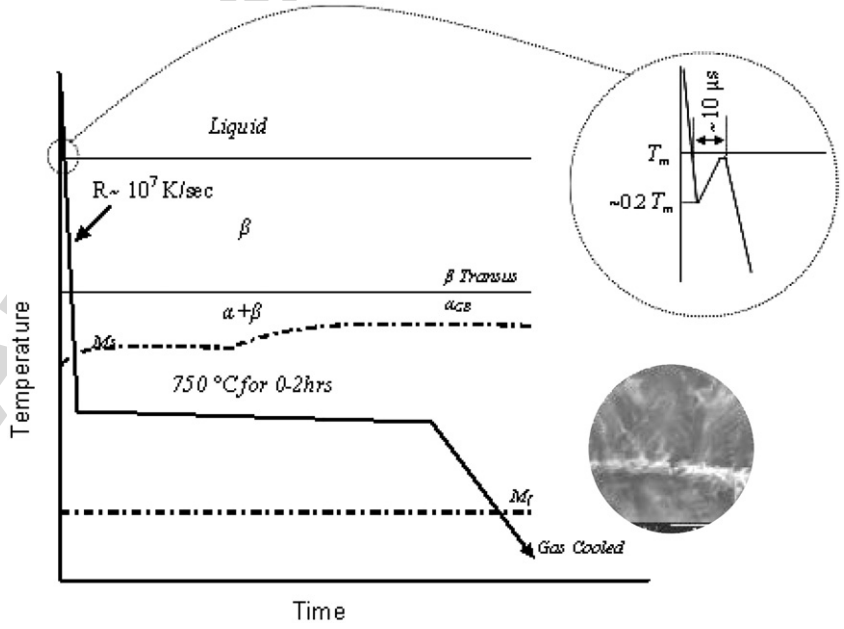

Fig. 6. A quantitative presentation of the cooling curve for a Ti–6Al–4V droplet during deposition.

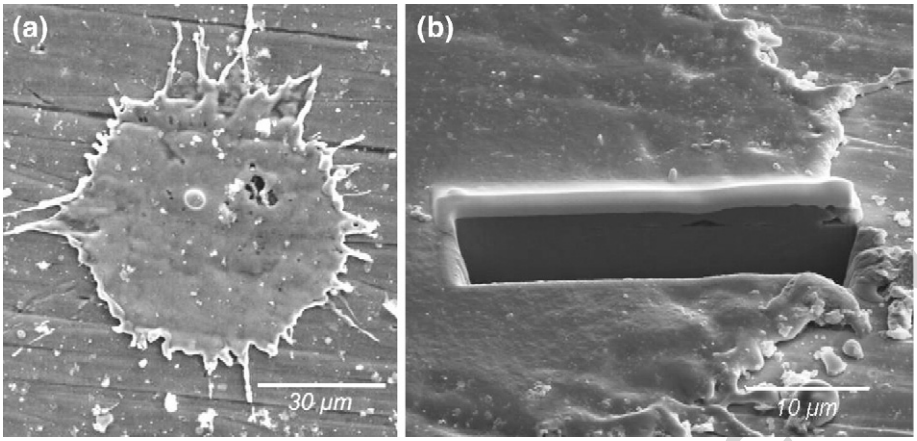

Fig. 7. SEM micrographs from a Ti–6Al–4V splat deposited on Ti substrate under vacuum plasma spray condition.

away from the centre of impact in the simulated images, see Fig. 2(b).

The solidification rate, R, can be also expressed as [4]:

$$R = \frac{h(T_t - T_s)}{\rho L_F} \quad (2)$$

where L_F is the latent heat of fusion (J kg^{-1}). The solidification front velocity is calculated to be 63 cm/s for a Ti–6Al–4V single splat under VPS conditions.

3. Experimental results

The cooling cycle of a single splat of Ti alloy is shown schematically in Fig. 6. After flattening and solidification, the splat cools down through the β phase region, of the phase diagram at a very high cooling rate, entering the α plus β region at the beta transus temperature. Because of the high cooling rate, the β transus temperature is shifted to a lower temperature compared to the equilibrium cooling condition.

Due to the absence of the convective cooling of deposits coupled with the high temperature of the incoming droplets and a strong interaction between the plasma jet and deposition, the temperature of the deposit was kept at a relatively high temperature (~ 800 °C in this study) during about 1 h over which deposition occurred. Therefore, self annealing of the deposit would be expected during spraying.

Fig. 7 shows SEM micrographs from top and cross section of a single splat of Ti–6Al–4V alloy impacted on Ti substrate under vacuum plasma spray condition. The cross section of the splat was made by Focused Ion Beam (FIB) milling (Micrion Corporation, Peabody, MA, USA). The splat curl up at the periphery and gap at the splat/substrate can be observed in the cross section. After the molten droplet impacts on the surface and spreads, it starts to solidify. While it cools down to the substrate temperature, shrinkage takes place through the already solidified material. If a portion of the splat/substrate is bonded, it cannot shrink while the upper side of the splat and periphery is free to interact. Therefore, tension stresses are created in the splat. The unbonded portion of the splat along with the periphery curls up to relieve the residual stresses [16].

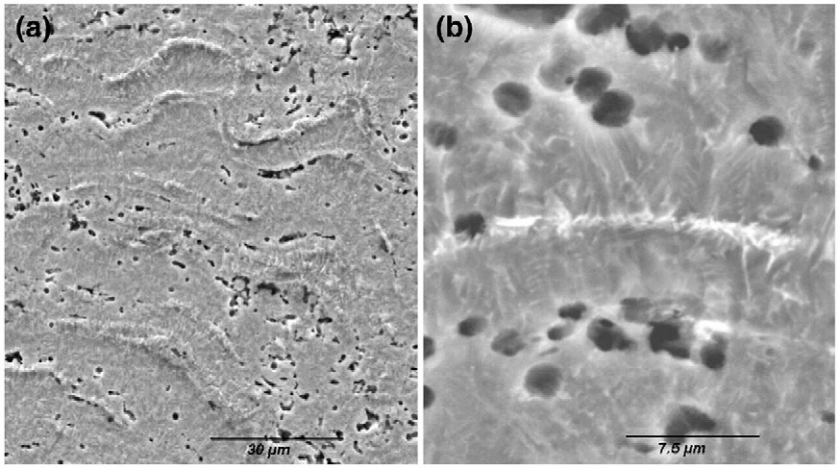

Fig. 8. SEM micrographs from cross section of the VPSF Ti–6Al–4V alloy. More deeply etched (gray) regions are the α′ lathes and small white regions are remnant β phase (b).

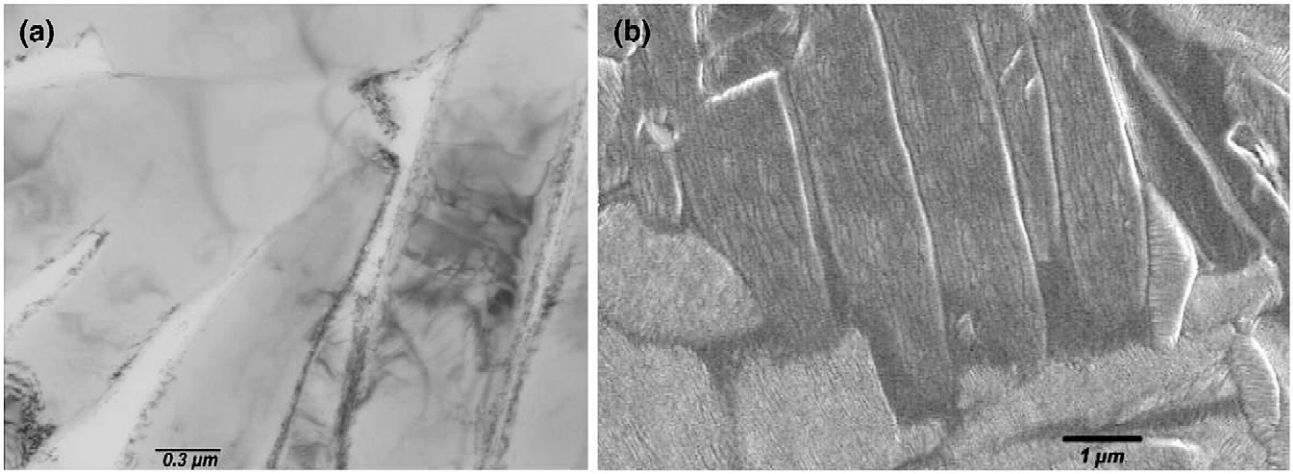

Fig. 9. (a) TEM and (b) SEM micrographs from the cross section of the VPSF Ti–6Al–4V structure show platelet and equiaxed grains.

Fig. 8 shows micrographs from the polished and etched cross section of the as-sprayed structure. The as-sprayed specimen was etched in Kroll's solution. More detailed descriptions about sample preparation were given in Refs. [17,18]. The as-sprayed microstructure indicates that the majority of the particles was molten at impact and had spread to produce good contact between the individual splats. The splat thickness was between 3 and 5 μm. The micrographs also show the columnar grain structure within the centre core of the splat oriented in the direction of the heat transfer into the prior splats. A magnified image (Fig. 8(b)) of a portion of Fig. 8(a) reveals the presence of two phases. The gray (more deeply etched) regions are the α′ lathes with a width about 0.5–1 μm, separated by small white regions of remnant β phase. The micrograph also indicates fusion across the lamellae boundaries. Some isolated pores within the splats and across the splat boundaries can be observed.

Because of the phase transformation of beta to martensite at the martensite formation temperature, M_s, after solidification, the original grain structure (prior β grains) formed during solidification cannot be observed clearly. The most frequently observed structures by Transmission Electron Microscope (TEM) and Scanning Electron Microscope (SEM) examinations from the lateral and cross sections show a herring-bone platelet structure and irregular-shaped fine equiaxed grains (see Fig. 9). Fig. 9(b) shows a SEM image of the as-sprayed structure after sputtering by Ga^+ ions for 2 h. The platelet length is in the range of 100 nm to 1 μm, and the width of the platelets is between 200 and 800 nm. The height of the columnar prior β grains is between 1 and 10 μm, which in some cases is more than the splat thickness (>4 μm). In this case, the columnar grains continued to grow in the top splat confirming superior cohesion between individual splats in the vacuum plasma spraying. Polygonized cells can also be observed within the equiaxed grains, indicating that recrystallization occurred during deposition. The high temperature of the molten particles during deposition and a strong interaction between the deposit and the flame during spraying lead to interdiffusion, self annealing, and recrystallization of deposits. Fine equiaxed grains are the result of self annealing and recrystallization of the deposit during spraying [4,14]. Sub-grain boundaries can be seen inside the α′ platelets. These grain boundaries can form during the recrystallization through rearrangement of dislocations, forming low angle grains and therefore reducing the residual stresses of the structure.

According to the cooling rate in the VPSF, a martensitic transformation to the metastable α′ martensite phase at M_s is likely. The X-ray diffraction pattern of the as-sprayed sample compared with the calculated reference patterns of both α-hexagonal and β-bcc titanium indicates the presence of α as the main phase along with the β-Ti as a minor phase in the specimen [17,18].

4. Conclusion

The cooling rate and solidification behavior of a single droplet of Ti–6Al–4V alloy under vacuum plasma spray conditions were studied numerically. The average cooling rate and solidification front velocity under interface-controlled heat transfer conditions were calculated to be 6×10^8 °C/s and 63 cm/s, respectively. The thermal contact resistance in the droplet/substrate interface was assumed to be zero (maximum heat transfer between the droplet and the substrate). However, the existence of inclusions, surface roughness and formation of micro gaps within the splat/substrate interface result in the thermal contact resistance at the interface and reduce the actual cooling rate of the splat. More studies on the effect of these parameters on the spreading behavior and solidification of thermal sprayed single splats have been reported elsewhere [19–22]. The experimentally measured cooling rate under vacuum plasma spray conditions for nickel was reported to be on the order of 10^7 °C/s [4], which is slightly lower than that obtained from the numerical results. Simulated results showed that solidification of a single splat was completed after 0.4 μs and approximately 30% of the initial droplet was splashed after solidification.

References

[1] S. Safai, F. Herman, Thin Solid Films 45 (1977) 295.
[2] M. Cohen, B.H. Kear, R. Mehrabian, in: R. Mehrabian, B.H. Kear, M. Cohen (Eds.), "Rapid Solidification Processing — An Outlook", Rapid

Solidification Processing: Principles and Technologies, vol. II, Louisiana, USA, 1980, p. 1.
[3] M. Cohen, R. Mehrabian, in: R. Mehrabian (Ed.), Some Fundamental Aspects of Rapid Solidification Processing: Principles and Technologies, vol. III, National Bureau of Standards, 1980, p. 1.
[4] S. Sampath, H. Herman, Journal of Thermal Spray Technology 5 (4) (1996) 445.
[5] M. Bussmann, J. Mostaghimi, S. Chandra, Physics of Fluids 11 (1999) 1406.
[6] M. Pasandideh-Fard, S. Chandra, J. Mostaghimi, International Journal of Heat and Mass Transfer 45 (2002) 2229.
[7] M. Bussmann, S. Chandra, J. Mostaghimi, Physics of Fluids 12 (2000) 3121.
[8] M. Pasandideh-Fard, V. Pershin, S. Chandra, J. Mostaghimi, Journal of Thermal Spray Technology 11 (2) (2002) 206.
[9] J.U. Brackbill, D.B. Kothe, C. Zemach, Journal of Computational Physics 100 (1992) 335.
[10] R. Boyer, G. Welsch, E.W. Collings (Eds.), Materials Properties Handbook: Titanium Alloys, 2nd ed, ASM International, Materials Park, OH, USA, 1998, p. 483.
[11] R. McPherson, Thin Solid Films 83 (1981) 297.
[12] D. Turnbull, Journal of Applied Physics 21 (1950) 1022.
[13] B. Cantor, R. Doherty, Acta Metallurgica 27 (1979) 33.
[14] R.C. Ruhl, Materials Science and Engineering 1 (1967) 313.
[15] P. Fauchais, Journal of Physics D: Applied Physics 37 (2004) 86.
[16] X. Xue, J. Mostaghimi, S. Chandra, in: B.R. Marple, et al., (Eds.), "Investigation of Splat Curling Up in Thermal Spray Coatings", Proceeding of the 2006 International Thermal Spray Conference, ASM International, Seattle, WA, USA, 2006.
[17] H.R. Salimijazi, T.W. Coyle, J. Mostaghimi, L. Leblanc, in: B.R. Marple, C. Moreau (Eds.), "Microstructural Formation of VPSF Ti–6Al–4V Alloys", ITSC (2003), Thermal Spray 2003: Advancing the Science and Applying the Technology, ASM International, Materials Park, OH, 2003, p. 611.
[18] H.R. Salimi Jazi, J. Mostaghimi, T. Coyle, JOM (2006) 50 (September).
[19] H.R. Salimi Jazi, J. Mostaghimi, T. Coyle, S. Chandra, C.Y. Lau, L. Rosenzweig, E. Moran, Journal of Thermal Spray Technology 16 (2) (2007) (June).
[20] J. Cedelle, M. Vardelle, P. Fauchais, Surface and Coating Technology 201 (2006) 1373.
[21] M. Fukumoto, H. Nagai, T. Yasui, in: B.R. Marple, et al., (Eds.), Influence of Surface Character Change of Substrate due to Heating on Flattening Behavior of Thermal Sprayed Particle, Proceeding of the 2006 International Thermal Spray Conference, ASM International, Seattle, WA, USA, 2006.
[22] X. Jiang, y. Wan, H. Herman, S. Sampath, Thin Solid Film 385 (2001) 132.